PERGAMON

International Journal of Heat and Mass Transfer 41 (1998) 3491–3500

International Journal of HEAT and MASS TRANSFER

Nucleate pool boiling of mercury in the presence of a magnetic field

Martin A. Lopez de Bertodano*, Sergio Leonardi, Paul S. Lykoudis

School of Nuclear Engineering, Purdue University, West Lafayette, IN 47907-1290, U.S.A.

Received 1 July 1997; in final form 14 January 1998

Abstract

This experiment is designed to investigate the fundamental mechanisms for pool boiling on a horizontal surface. The unique feature is the combination of an artificial re-entrant cavity and a multiple sensor conductivity probe located above it. With this arrangement the bubble size and frequency were measured. Furthermore, the number density of the nucleation sites is prescribed (i.e. the single re-entrant cavity built into the heater surface). These basic data were not previously available for liquid metals with magnetic fields.

The most striking result is the suppression of boiling at high values of the magnetic field. Good agreement between the data and a mechanistic model were obtained provided that the bubble frequency was known. The effect of the magnetic field on the bubble frequency needs to be resolved for closure.

1. Introduction

Whereas a lot of research has been done on boiling of various fluids [1], including liquid metals [2], not much work exists on Magneto-hydrodynamic (MHD) boiling. However this phenomenon may play an important role in the blanket design of future fusion reactors.

Some theoretical aspects of MHD boiling have been addressed by Lykoudis [3] who defined a magnetic interaction number to extend the classical Rayleigh problem of bubble growth in the presence of a magnetic field. Lykoudis [4] was able to correlate MHD pool boiling data [5] based on this theoretical result in combination with Forster and Zuber's correlation [6]. The data were obtained with boiling mercury on a horizontal plate in the presence of a horizontal magnetic field—up to 1.25 tesla. A similar experiment [7], up to 7 tesla, produced analogous results. Lykoudis and Takahashi [8] obtained local measurements for the bubble frequency which increased with the magnetic field up to 0.6 T; however, at low heat fluxes, the frequency decreased beyond that value.

The state-of-the-art in MHD boiling is far behind the mechanistic models presently available for pool boiling heat transfer because there are no data to validate such models.

2. Theoretical models

There is a general consensus that discrete bubble pool boiling is a sum of bulk convection caused by the bubbles and natural convection [9, 10]. The mechanistic model by Han and Griffith [9] will be used in this study. The heating surface in pool boiling is considered to be divided into two parts: the bulk convection area and the natural convection area. In the area of bulk convection, heat is assumed to be transferred into the fluid by transient conduction. Following the departure of a bubble from the heating surface, a piece of superheated liquid is brought into the main body of the fluid. In the area where natural convection occurs, heat is supposed to be transferred from the heated wall to the main body of the fluid by the usual convection process in a continuous manner.

2.1. Natural convection

This process has been widely studied for the last century and is well understood. When the magnetic field

* Corresponding author. E-mail: bertodan@ecn.purdue.edu

0017-9310/98 $19.00
PII: S0017-9310(98)00046-5

effects are included, the problem becomes more complicated. Lykoudis [11] examined the case of a vertical hot plate surrounded by an electrically conducting fluid in the presence of a horizontal magnetic field. He showed that a similarity solution existed which was dependent upon a single non-dimensional number:

$$Ly = \frac{\sigma_e B^2 \sqrt{L}}{\rho_f \sqrt{g\beta\Delta T}}, \tag{1}$$

where B is the magnetic flux density, L is a characteristic length, ρ_f is the density of the liquid, g is the gravitational constant, β is the thermal expansion coefficient and ΔT is the temperature difference between the wall and the bulk.

At a later date, this theoretical conclusion was verified experimentally [12, 13]. In the present case, where a horizontal rather than vertical heated plate is used, a theoretical model for natural circulation was not developed. The correlation for a horizontal plate was determined by Wagner and Lykoudis [6]:

$$\frac{Nu_B}{Nu_0} = \frac{21.2\sqrt{Pr}}{\sqrt{4.5+Ly}}, \tag{2}$$

where Nu_0 was calculated using the correlation by Globe and Dropkin [14] with a modification for the aspect ratio, H/D, of the liquid pool recommended by Chiesa and Guthrie [15]:

$$Nu_0 = 0.078(0.68)^{H/D} Pr^{0.074} Ra^{1/3} \tag{3}$$

2.2. Boiling

In the area occupied by bubbles, heat is assumed to be transferred into the fluid by a transient conduction process. Following the departure of a bubble from the heated surface, a piece of superheated liquid is brought into the main body of the fluid (the bulk of the fluid). This is a periodic removal of the thermal boundary layer, and it is repeated with f, the bubble departure frequency. By this kind of repeated process, heat is transferred into the main body of the fluid.

In what follows we summarize Han and Griffith's model [9]. If n is the number of active nucleation sites per unit area, then the total heat removal by the bulk convection of the thermal boundary layer is approximately

$$q''_{BC} = nf\Delta Q, \tag{4}$$

where ΔQ is the heat transferred to the boundary layer during the bubble formation cycle. Assuming a doughnut-shaped layer around the bubble,

$$\Delta Q = 2\rho_f c(T_w - T_{sat})[R_i^2\delta_d - \tfrac{1}{3}R_d^2(\delta_d - \delta_c)], \tag{5}$$

where c is the specific heat of the fluid, R_d is the bubble radius at departure, R_i is the influence radius ($R_i = 5R_d$ was used in the present calculations), δ_d is the boundary layer thickness at departure and δ_c is the boundary layer thickness at the end of waiting time.

By treating the liquid adjacent to the surface as a solid slab and solving the transient conduction problem:

$$\delta_d = \sqrt{\frac{\pi\alpha}{f}}, \tag{6}$$

$$\delta_c = \sqrt{\pi\alpha t_w}, \tag{7}$$

where α is the thermal diffusivity of the liquid.

During the waiting time, the bubble radius R_c remains approximately constant and the bubble surface is isothermal and adiabatic. The waiting time, t_w, can then be obtained using potential flow theory and the fluid flow analogy:

$$t_w = \frac{9}{4\pi\alpha}\frac{(T_w - T_{sat})R_c}{T_w - T_{sat}\left[1 + \left(\frac{2\sigma}{R_c\rho_g h_{fg}}\right)\right]}, \tag{8}$$

where R_c is the cavity radius, T_w is the wall temperature, σ is the surface tension, ρ_g is the vapor density and h_{fg} is the latent heat of vaporization.

By combining equations (4) and (6), we obtain

$$q''_{BC} = nf2\rho_f c(T_w - T_{sat}) \times \left[4R_d^2\sqrt{\frac{\pi\alpha}{f}} - \frac{1}{3}R_d^2\left(\sqrt{\frac{\pi\alpha}{f}} - \sqrt{\pi\alpha t_w}\right)\right]. \tag{9}$$

Note that equations (8) and (9) allow to compute 'mechanistically' the heat flux when measuring temperatures, bubble frequency and departure size, and cavity radius. This model has been used in the present work together with equation (3). It is assumed natural convection occurs over the surface of the plate beyond the region of influence of the cavity:

$$q''\pi R_h^2 = q''_{BC}\pi R_i^2 + q''_{NC}\pi(R_h^2 - R_i^2) \tag{10}$$

where R_h is the radius of the heated plate. The frequency of bubble nucleation and the size of the bubbles remain to be modeled. In this work the measured values are used. However the effect of the magnetic field on these quantities is significant and at present it remains unknown. Lykoudis' [4] considered the slowing down effect of the magnetic field on the growth rate of the bubbles:

$$\frac{q''_B}{q''_0} = \frac{1}{(1+\sqrt{\Lambda})^{2.44}} \tag{11}$$

where q''_0 is the pool boiling heat flux without the magnetic field calculated with Forster and Zuber's model [6], q''_B with the magnetic field, and Λ is a non-dimensional number defined as [3]:

$$\Lambda = \frac{\sigma_e B^2 \alpha}{\Delta p}\left[\frac{\rho_f C_p(T_w - T_{sat})}{\rho_g h_{fg}}\right]^2 \tag{12}$$

where σ_e is the electrical conductivity, B is the magnetic field, α is the thermal diffusivity, and Δp is the pressure

difference across the interface. However equations (11) and (12) are an integral correlation and it would be desirable to obtain physical models for the effects of the magnetic field on the bubble frequency and the bubble size that are inputs to equation (9).

3. Experiment

3.1. Apparatus

Many previous experiments have been performed at our laboratory. Wagner and Lykoudis [5] obtained the first set of data shown in Fig. 1. The preparation of the boiling surface presented special difficulty because of the large contact angle of mercury, but they succeeded to obtain repeatable nucleate boiling data using a sand-blasted surface. Later a double conductivity probe was developed, capable to withstand the high temperature environment of boiling mercury, to measure bubble frequency and velocity. Lykoudis and Takahashi used this probe and obtained the bubble frequency data shown in Fig. 2. They observed that the bubble frequency increased with B initially, and later decreased.

With the combination of the double conductivity probe and the re-entrant cavity, it is possible to obtain the bubble frequency, the bubble size and the nucleation site density that are required by equation (9). Schematics of the experimental apparatus are shown in Figs 3 and 4. The design is based on a previous experiment [5]. The mercury boiling vessel consists of a vertical stainless steel cylinder 60 mm in diameter and 460 mm tall with a condenser near the top. An external concentric stainless steel tube is filled with silicon oxide powder for insulation (conductivity = 0.07 W/m K). To reduce heat losses even further the boiler assembly is insulated on the outside with a rectangular block of Marinite (conductivity = 0.124 W/m K). The minimum thickness of the outer insulation is 40 mm.

There are two vacuum pumps connected to the system, one to each cylinder. The primary pump connected to the boiler set the system pressure and the other pump maintained a low pressure in the annulus to prevent mercury leaks to the laboratory. Cold traps were installed

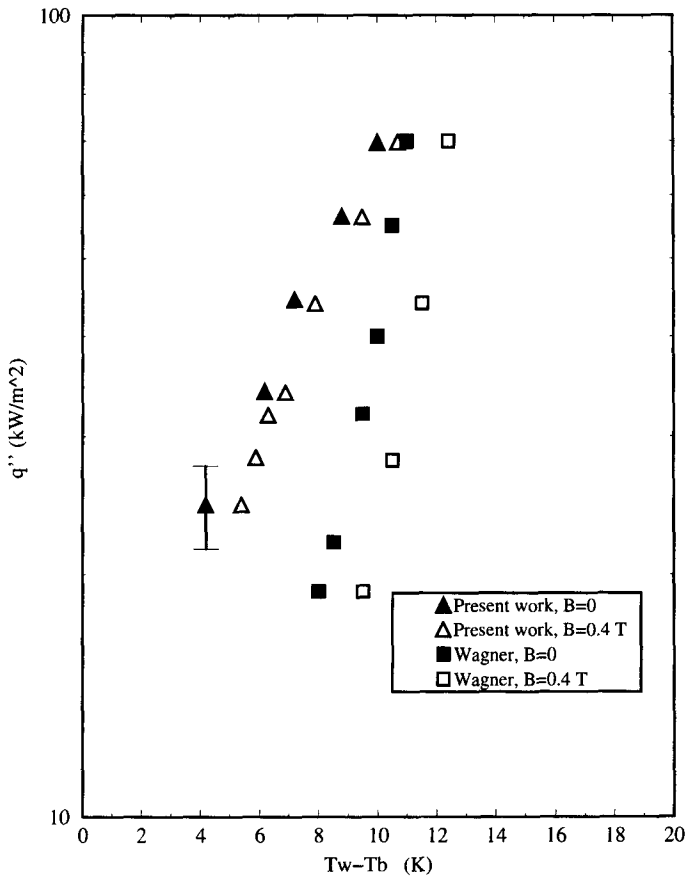

Fig. 1. Comparison of present data with boiling curves of Wagner and Lykoudis [5].

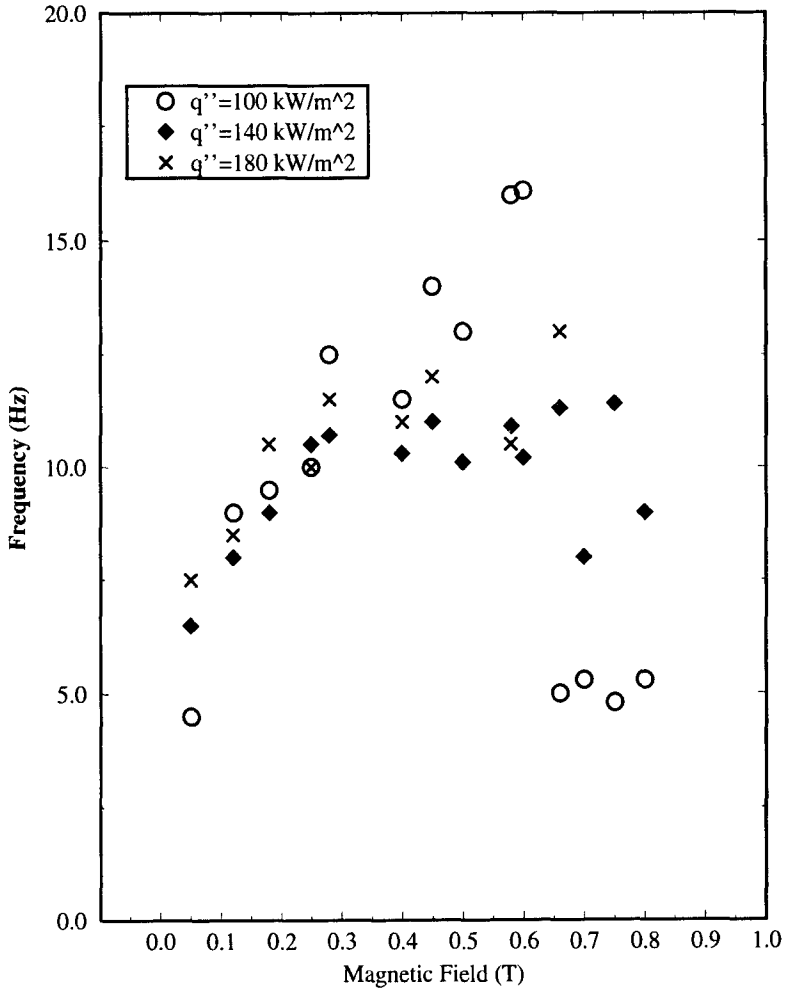

Fig. 2. Bubble frequency data of Lykoudis and Takahashi vs Magnetic field [8].

between the vacuum pumps and the boiler to condense the mercury vapor extracted from the system.

The experimental apparatus was inserted in the 178 mm gap between the pole faces of the 1 tesla electromagnet. The large surface area of the electromagnet faces (1 m by 0.3 m) provide a uniform horizontal magnetic field within the small volume of the boiling experiment.

The 60 mm stainless steel heater has a maximum power of 1000 W. The surface was polished in three stages to obtain a mirror like finish (Fig. 5) to prevent nucleation sites other than the artificial cavity. One artificial reentrant cavity was machined in the center of the heater (Fig. 6). First a 6.4 mm hole was drilled, then it was plugged and the polishing was performed. Finally a 0.8 mm hole was drilled in the center of the plug.

The measurements consisted of heater power and temperature, bulk temperature, and the double conductivity probe. The power was measured with a voltmeter and an ammeter. The heater temperature was measured with a 25 mm long calibrated resistance temperature detector (RTD) inserted horizontally 2 mm below the surface. Bulk mercury temperatures were measured with two calibrated J-type thermocouples.

The double conductivity probe consists of two point electrodes located in the vertical axis and 2 mm apart. The circuits have a 15 V DC power supply and a 10 kΩ resistor in series. The stainless steel boiler vessel completes the circuits. The conductivity probes measure the phase indicator function (i.e. 0 volts when the tip is immersed in the liquid phase and 15 volts for the vapor phase). The output voltages of the point electrodes were digitized at 5000 Hz and stored in a PC.

3.2. Procedure

The purity of the mercury was crucial to obtain consistent data. Quadruple-distilled mercury was used. The boiler was evacuated of air with the primary vacuum

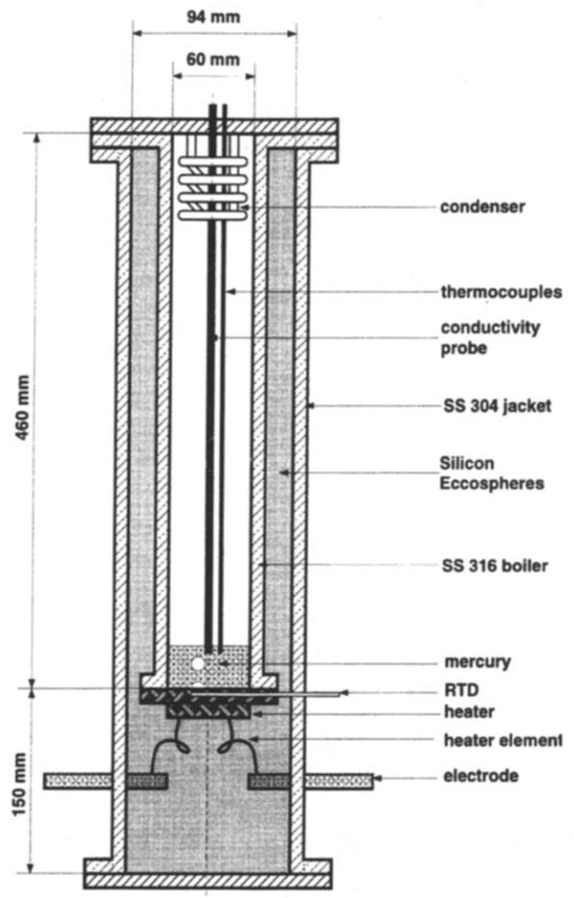

Fig. 3. Schematic of MHD boiling test section.

pump and then filled with 99.99% nitrogen cover gas to prevent oxidation. This procedure was repeated twice.

An aging procedure was followed to obtain wetting of the surface by the mercury. The initial data (i.e. high wall temperature and very low bubble frequency) indicated that film boiling was taking place. This is a non-wetting effect that has been reported previously. However after 48 h of continuous boiling at a low heat flux of 35 kW/m^2 all indications of film boiling disappeared. A glass top was used to ensure visually that stable nucleate boiling was obtained and that the only active site was the re-entrant cavity.

The bubble frequency was measured with the conductivity probe 2 mm above the cavity to capture all the bubbles. The probe was positioned 15 mm above the cavity to measure the bubble size. This distance is large enough for the bubbles to reach their terminal velocity. The theory of the double conductivity probe measurement has been previously developed [16, 17]. Assuming that the probe passes every point of the bubble surface with equal probability, that the velocity fluctuations are random and that the vertical component of the velocity is larger than the horizontal fluctuations the interfacial area concentration is given by:

$$a_i = 4f\frac{\bar{1}}{|v_i|}\frac{\phi_0}{\sin\phi_0} \tag{13}$$

where the bubble frequency was computed as one half of the interface impact rate. The interfacial velocity, v_i, was computed as the distance between the two conductivity probes divided by the time between the two signals. The dependence on ϕ_0 is a correction for the distribution of angles between the bubble trajectories and the axis of the double conductivity probe where ϕ_0 is calculated from the implicit relation:

$$\frac{\sin(2\phi_0)}{2\phi_0} = \frac{1-\sigma_z^2/v_i^2}{1+3\sigma_z^2/v_i^2} \tag{14}$$

where σ_z is the standard deviation of the component of the interfacial velocity fluctuations along the axis of the probe. Finally the Sauter mean diameter is calculated as $D = 6a_i/\alpha$ where α is the vapor fraction or the time fraction of the vapor phase measured by the leading conductivity probe.

The data were obtained at atmospheric pressure and the mercury level was 30 mm.

3.3. Uncertainty analysis

The theoretical model described by equations (2), (3), (9) and (10) was used for the standard error propagation analysis. The result of the calculations is displayed as error bars in the plots. The relevant sources of the error were identified as the magnetic field, B, the heater and bulk liquid temperatures, T_h and T_B, the bubble radius, R_b, the radius of influence, R_i. And the bubble frequency, f. The individual uncertainties are listed in Table 1.

It was difficult to provide an estimate of the errors for the bubble data. The error in the bubble diameter was assumed to be 2 mm which corresponds to the distance between the tips of the double conductivity probe. The error in the frequency was assumed to be 2 Hz, which is a conservative estimate based on the comparison between video recorded data and probe data.

Table 1

Variable	Error	Obtained from
B	0.05 T	existing calibration
T_h	0.1 K	manufacturer calibration
T_B	0.5 K	manufacturer calibration
R_b	1 mm	distance between electrodes
R_i	$1/2R_b$	estimate
f	2 Hz	estimate

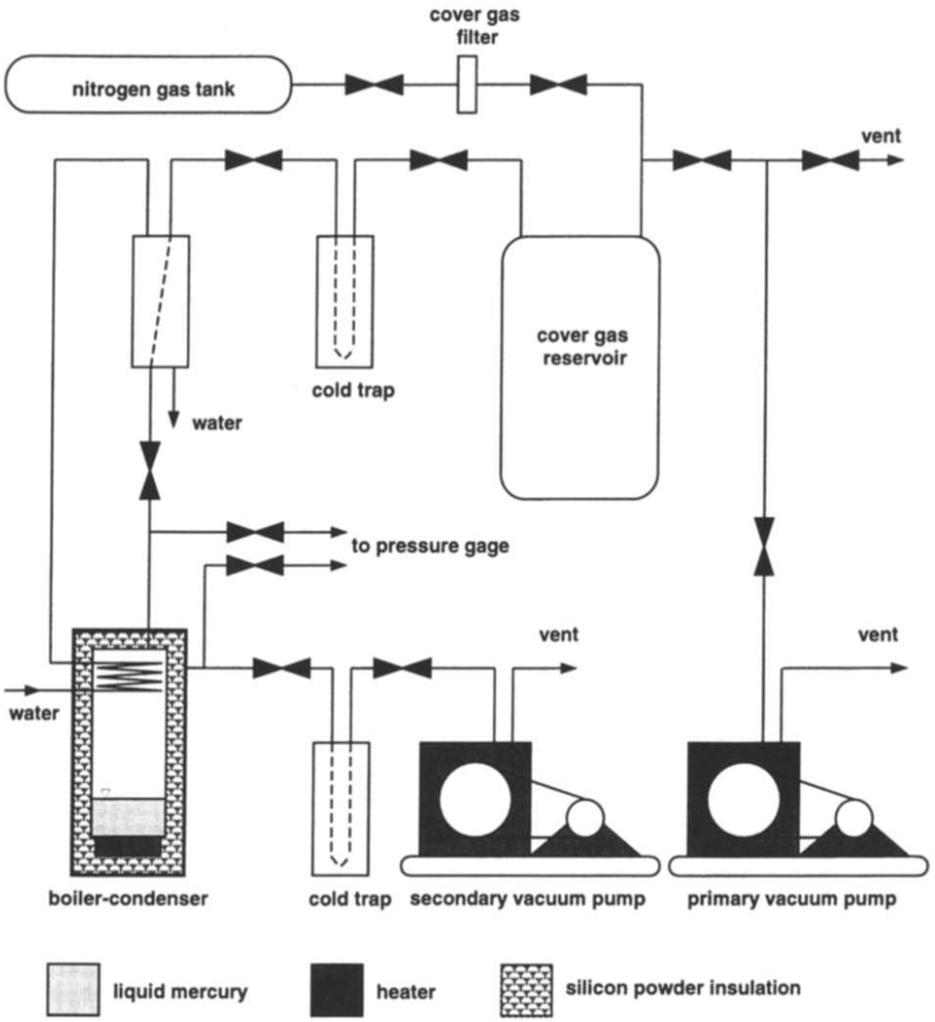

Fig. 4. Schematic of apparatus.

4. Results

Figure 1 shows a comparison between the present experiment and previous boiling data. The effect of the magnetic field is the same in both experiments but the heater surfaces are different so the boiling curves are different.

Figure 7 shows a comparison of the single phase natural circulation data with equation (2). The effect of the magnetic field is exhibited most strongly at low values of the Ly number, where the heat transfer decreases sharply. The data of Wagner and Lykoudis [5] show a similar trend with the new data but the suppression of heat transfer is greater, partly because they used a different depth of mercury (i.e. 40 mm vs 30 mm).

The measured bubble velocities are shown in Fig. 8. For $B < 0.5$ T the velocities do not change with the magnetic field and are between 0.2 and 0.3 m/s. However for $B > 0.5$ T the velocities increase slightly. The bubble sizes calculated from equation (13) and the measured velocities are shown in Fig. 9. The bubble size increases with the heat flux and also to a lesser degree with the magnetic field.

Figure 10 illustrates the effect of the magnetic field on the bubble frequency. The results are similar to previous data shown in Fig. 2. The frequency increases with a moderate increase in the magnetic field up to 0.4 T. The qualitative explanation is that the convection is slowed down by the magnetic field so the thermal boundary layer becomes thicker to the point where the temperature of the bubble induced flow that rewets the wall is greater. Therefore the waiting between bubbles decreases. How-

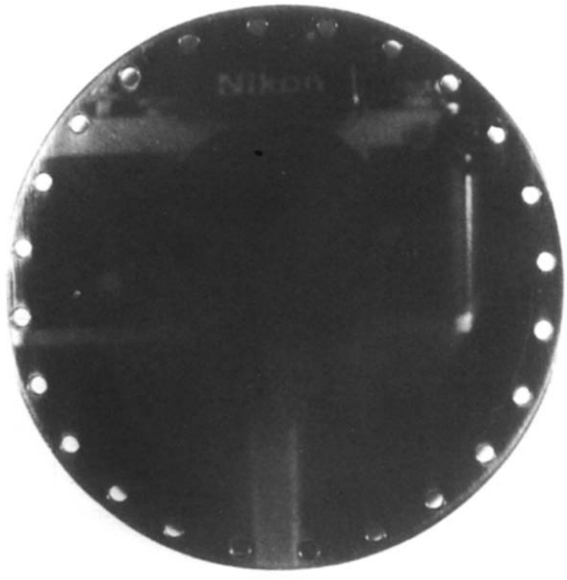

Fig. 5. Photograph of heater.

ever the experimental data show that the bubble frequency *decreases* with further increases of the magnetic field. This result is strongest for the low heat fluxes, causing the bubbles to disappear completely at the lowest heat flux. The reason for this is not clear.

Calculations were done with equations (2), (3), (9) and (10) to obtain the total heat flux and compared with the present data. The biggest uncertainty in the model was the bubble size. This deviation in the data causes a large difference in the predictions as shown by the upper and lower curves in Figs 11 and 12. However the data does fall within the error bounds and the slopes are in agreement too.

Figure 12 shows the effect of 'bumping' which has been previously observed in liquid metals. At low heat fluxes and high magnetic fields stable nucleate boiling could not be sustained. Instead boiling was suppressed and the heater temperature would gradually increase until a boiling burst occurred. At this point the temperature dropped rapidly and the process was repeated. The lower part of the boiling curve in Fig. 12, which curves backwards, coincides with the bumping process. For the lowest heat flux datum boiling was completely suppressed. This effect only occurred when the magnetic field was greater than 0.5 T. Leonardi's heat transfer data [18] show the same trend for the four magnetic fields from 0.6 T to 0.9 T. This can also be seen in Figure 10 where the bubble frequency is zero for the same four cases.

5. Conclusion

In the present work a special heater surface with a re-entrant artificial cavity was developed for mercury pool boiling in the presence of a magnetic field. With this heater and the double conductivity probe a new set of data were obtained that may be used to develop a mechanistic model.

The data were correlated satisfactorily with the mech-

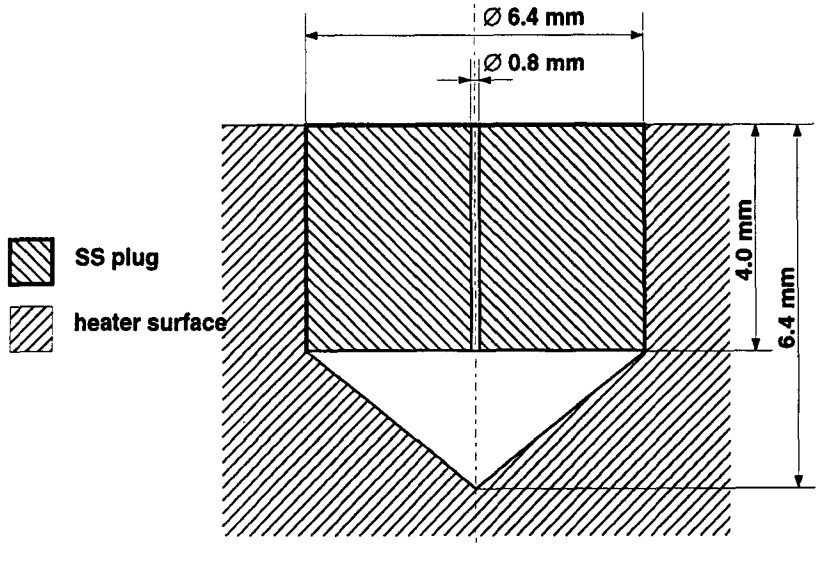

Fig. 6. Artificial re-entrant cavity geometry.

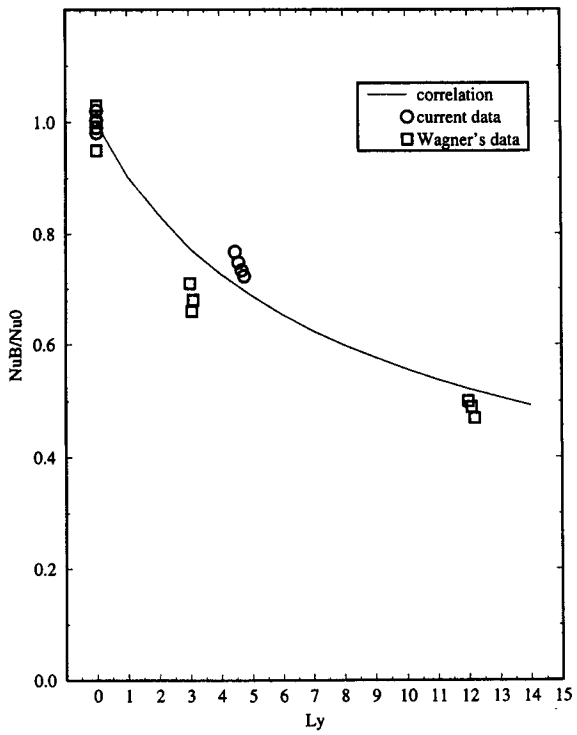

Fig. 7. Natural convection data for single phase flow vs equation (2).

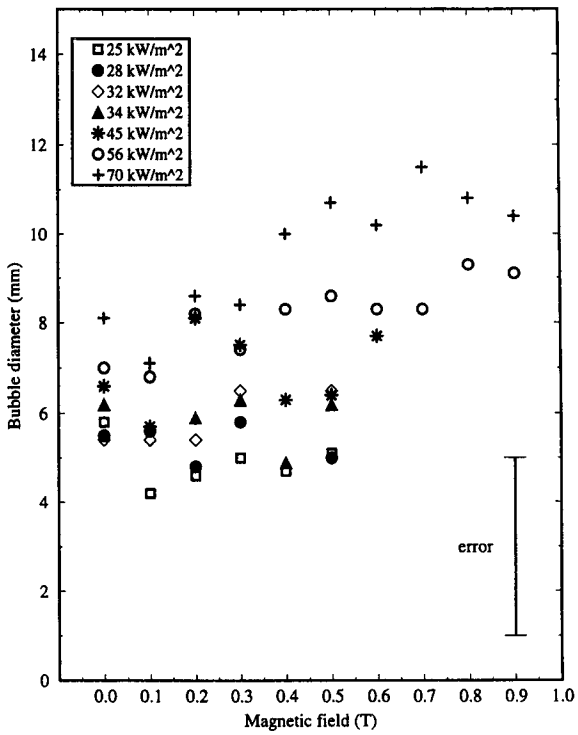

Fig. 9. Effect of the magnetic field on the bubble size data.

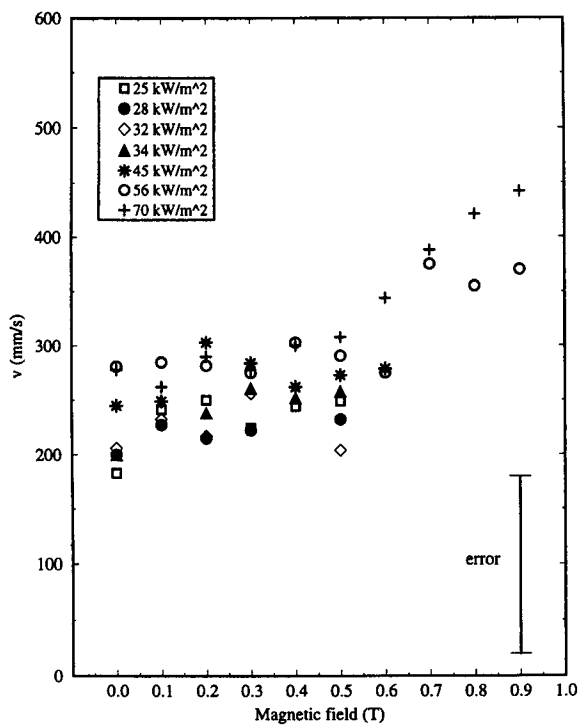

Fig. 8. Effect of the magnetic field on the bubble rise velocity data.

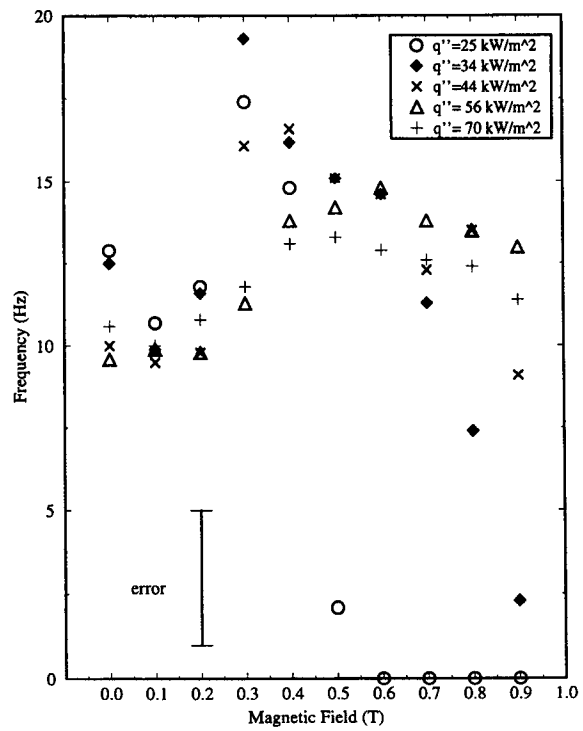

Fig. 10. Effect of the magnetic field on the bubble frequency data.

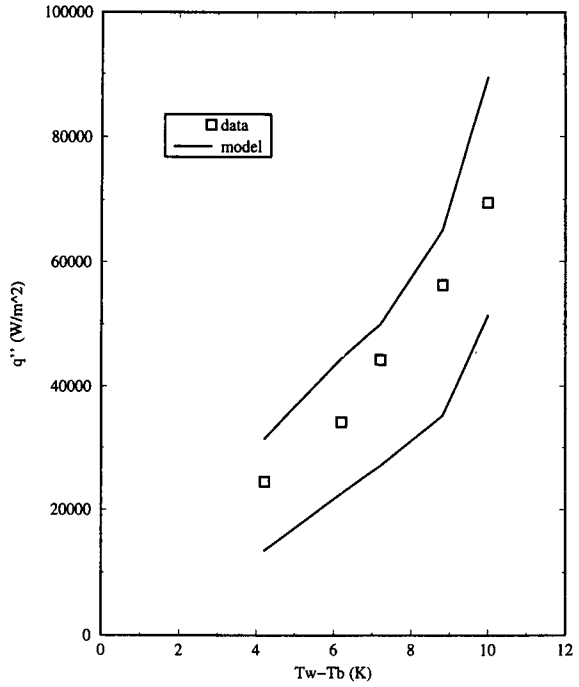

Fig. 11. Comparison of the heat flux data with mechanistic model ($B = 0$ T).

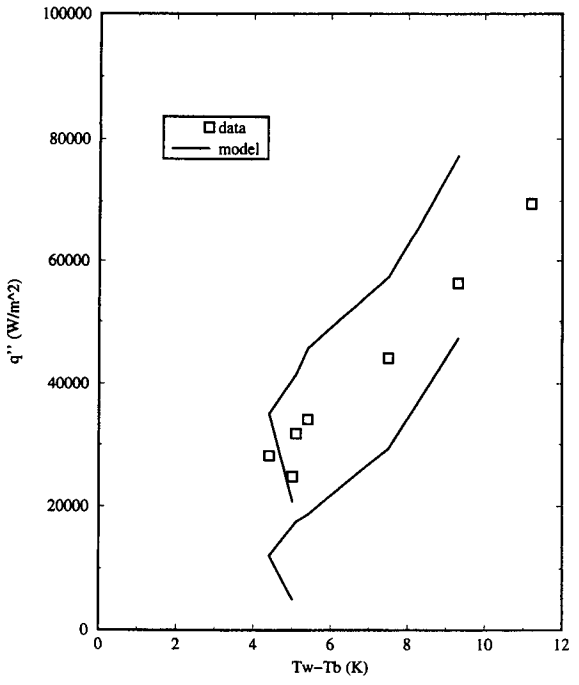

Fig. 12. Comparison of heat transfer data with mechanistic model ($B = 0.6$ T).

anistic model by Han and Griffith [9]. However this is not a predictive model because the bubble size and frequency were prescribed (i.e. the data were used). Whereas the effect of the magnetic field on the bubble size was not very significant, the effect on the bubble frequency was to first increase the bubble frequency and then to produce suppression of boiling. For the lowest heat flux data the suppression was complete when $B < 0.6$ T. A physical model for the effect of the magnetic field on the bubble frequency is still missing.

References

[1] Fujita Y. The state-of-the-art nucleate boiling mechanism. Proceedings of the Engineering Foundation Conference on Pool and External Flow Boiling, ASME, Santa Barbara, California, March 22–27, 1992, pp. 83–98.

[2] Michiyoshi I. Boiling heat transfer in liquid metals. Appl Mech Rev 1988;4(3):129–48.

[3] Lykoudis PS. Bubble growth in the presence of a magnetic field. Int J Heat Mass Transfer 1976;19:1357–62.

[4] Lykoudis PS. Bubble growth in a superheated liquid metal in a uniform magnetic field. Proceedings of the Fourth Beer-Sheva International Seminar on Magneto-hydrodynamic Flows and Turbulence, Ben-Gurion University of the Negev, Beer-Sheva, Israel, February 27 to March 2, 1984, pp. 280–303.

[5] Wagner LY, Lykoudis PS. Mercury pool boiling under the influence of a horizontal magnetic field. Int J Heat and Mass Transfer 1981;24(4):635–43.

[6] Forster K, Zuber N. Dynamics of vapor bubbles and boiling heat transfer. American Institute of Chemical Engineers Journal 1976;1(4):425–9.

[7] Takahashi O, Nishida M, Takenaka N, Michiyoshi I. Pool boiling heat transfer from horizontal plane heater to mercury under magnetic field. Int J Heat Mass Transfer 1980;23:27–36.

[8] Lykoudis PS, Takahashi M. Nucleate boiling of mercury in the presence of a horizontal magnetic field. In Metallurgical Technologies, Energy Conversion and MHD Flows, ed. H Branover and Y Unger, AIAA, 1993;148:626–34.

[9] Han CY, Griffith P. The mechanism of heat transfer in nucleate pool boiling—Parts I and II. Int J Heat Mass Transfer 1965;8:887–913.

[10] Mikic BB, Rohsenow WM. A new correlation of pool-boiling data including the effect of heating surface characteristics. Trans ASME, J Heat Transfer 1969;91:245–50.

[11] Lykoudis PS. Natural convection of an electrically conducting fluid in the presence of a magnetic field. Int J Heat Mass Transfer 1962;5:23–34.

[12] MacGregor RJ, Lykoudis PS. Natural convection experiment with mercury in a transverse magnetic field, Technical Report 64-9, School of Aeronautics and Astronautics, Purdue University, 1964.

[13] Papailiou D. Magneto-fluid-mechanic turbulent free con-

vection flow. Ph.D. Thesis, School of Nuclear Engineering, Purdue University, 1971.

[14] Globe S, Dropkin D. Natural convection heat transfer in liquids confined by two horizontal plates and heated from below. Trans ASME, J Heat Transfer 1959;81:24–8.

[15] Chiesa F, Guthrie R. An experimental study of natural convection and wall effects in liquid metals contained in vertical cylinders. Met Trans 1971;2:2833–8.

[16] Kataoka I, Ishii M, Serizawa A. Local formulation and measurements of interfacial area X concentration in two-phase flow. Int J Multiphase Flow 1986;12(4).

[17] Wu Q, Zheng D, Ishii M, Beus S. Measurements of interfacial area concentration in two-phase flow with a two point conductivity probe, submitted to Int J Multiphase Flow 1977.

[18] Leonardi S. Liquid metal heat transfer in a magnetic field, M.S. Thesis, School of Nuclear Engineering, Purdue University, December 1996.